Journal of Solid State Chemistry **147,** 74–81 (1999)
Article ID jssc.1999.8176, available online at http://www.idealibrary.com on IDEAL®

Intercalation of Hexagonal Boron Nitride by Strong Oxidizers and Evidence for the Metallic Nature of the Products[1,2]

Ciping Shen,* Steven G. Mayorga,* Richard Biagioni,* Charles Piskoti,† Masahiro Ishigami,† Alexander Zettl,† and Neil Bartlett*

*Chemistry Department, †Physics Department, and Chemical Sciences and Materials Sciences Divisions, Lawrence Berkeley National Laboratory, The University of California at Berkeley, Berkeley, California 94720

Received November 9, 1998; in revised form January 20, 1999; accepted January 21, 1999

Hexagonal boron nitride, *h*-BN, is intercalated, at $\sim 20°C$, by $S_2O_6F_2$ (the source of the powerfully oxidizing $SO_3F^{\bullet}$ radical) to give a deep blue solid $(BN)_{\sim 3}SO_3F$, which is a temperature-independent paramagnet ($x_g \approx 55.2 \times 10^{-6}$ cgs units). Four probe conductivity measurements on an intercalated piece of highly oriented pyrolytic BN (HOPBN) have established an approximate doubling of the conductivity with temperature decrease from 295 to 77 K. The low conductivity ($\sigma_{295K} = 1.5\ S\ cm^{-1}$) is attributed to high effective carrier mass deriving from poor $p\pi_N - p\pi_B$ overlap and consequent narrow band character. The conductivity at 295 K of a graphite relative of composition $C_{\sim 8.5}SO_3F$ made from a HOPG chip was found to be $1.1 \times 10^5\ S\ cm^{-1}$, and at 77 K it was found to be $3.1 \times 10^5\ S\ cm^{-1}$. Other blue, poorly conductive *h*-BN intercalation compounds have been obtained using SbF_5/F_2 mixtures on *h*-BN, and from AsF_5 on $(BN)_{\sim 3}SO_3F$, but they are of unknown composition.

Key Words: **boron nitride; intercalation; metallic; oxidation.**

INTRODUCTION

Hexagonal boron nitride, *h*-BN, is isoelectronic with graphite and their structures are similar (1) (graphite: $a = 2.464$, $c = 6.708$; *h*-BN: $a = 2.504$ Å, $c = 6.660$ Å) except for the difference in the stacking of the layers. In *h*-BN, because of its partial ionic character, the B and N atoms in neighboring sheets eclipse each other, and this gives rise to an interaction between the sheets stronger than that in graphite, where adjacent sheets are staggered and only half of the C atoms in any one sheet eclipse C atoms in adjacent layers.

Although Croft (2) had claimed a variety of intercalation compounds, involving *h*-BN and transition metal halides such as $FeCl_3$, those claims were contested by Rudorff and Stumpp (3). Freeman and Larkindale (4, 5) reported that a pink product from the interaction of *h*-BN with $FeCl_3$ was accompanied by a small expansion of the interlayer spacing, but Ohashi and Shinjo (6) made an extensive study of this system and concluded that the pink material was due to a surface hydrolysis product, FeOCl. Reductive intercalation of *h*-BN by alkali metals has also been claimed, (7) but not substantiated (8).

Nearly 20 years ago, from these laboratories, a dark blue boron nitride fluorosulfate, $(BN)_4SO_3F$, and a graphite relative, $C_{12}SO_3F$, were briefly described, and each was reported (9) to be an electrical conductor. Hooley, however, failed (10) to confirm these observations for the *h*-BN salt. The thermodynamic instability of the $(BN)_xSO_3F$ with respect to BF_3 and other products had been noted in the original report (9). Subsequent work (11–13) in these laboratories found wide variations in the room-temperature stability of the product.

This paper describes the conditions for the synthesis of dark blue first-stage material which has long-term stability at $\sim 20°C$. It has composition $(BN)_{\sim 3}SO_3F$. The magnetic susceptibility and electrical conductivity behavior are described and found to be consistent with that of a metal. Powdered samples of $(BN)_{\sim 3}SO_3F$ and $C_{\sim 7}SO_3F$ are compared. Other first-stage intercalation compounds of *h*-BN have been derived from the action of AsF_5 on $(BN)_{\sim 3}SO_3F$ or by direct interaction of *h*-BN with liquid SbF_5 and F_2 gas, but they are of uncertain composition.

EXPERIMENTAL

Reagents. *h*-BN powder (Ventron, Beverly, Ma) was used in the synthesis of powder samples of $(BN)_{\sim 3}SO_3F$. Highly oriented pyrolytic boron nitride (14) (Union Carbide), HOPBN, was used to prepare $(BN)_{\sim 3}SO_3F$ for the conductivity measurement. The *h*-BN powder and HOPBN were degassed under a dynamic vacuum of 10^{-6} Torr,

[1]Dedicated to the memory of Jean Rouxel, a first-rank scientist and friend.

[2]The U.S. Government's right to retain a nonexclusive royalty-free license in and to the copyright covering this paper, for governmental purposes, is acknowledged.

0022-4596/99 $30.00

heated occasionally with a gas flame. XeF_2 was prepared photochemically according to the literature method (15). HSO_3F (Allied Chemical Co., Morristown, NJ) was distilled and stored in a Pyrex vessel with a break-seal prior to use. Peroxydisulfuryl difluoride, $S_2O_6F_2$, was prepared (16) via the interaction of XeF_2 and HSO_3F,

$$XeF_2 + 2HSO_3F \rightarrow Xe(SO_3F)_2 + 2HF, \qquad [1]$$

and the subsequent decomposition of $Xe(SO_3F)_2$ in a Pyrex glass vessel with a greaseless J. Young glass–Teflon valve ensured that the $S_2O_6F_2$ was free of HF.

$$Xe(SO_3F)_2 \rightarrow S_2O_6F_2 + Xe \qquad [2]$$

X-ray powder diffraction photographs. The quartz capillaries used for X-ray powder diffraction studies were dried under vacuum (10^{-6} Torr) at 1070 K for 24 h before being transferred to the dry Ar atmosphere of a Vacuum Atmospheres Corporation DRILAB. X-ray powder samples were prepared as previously described (17). Photographs were taken using a 45-cm-circumference G.E. camera with Straumanis loading, the radiation being Cu$K\alpha$ with a nickel filter.

Preparation of $(BN)_{\sim 3}SO_3F$. Whenever preparations were carried out in apparatus with base-metal (e.g., Fe or Ni) components (11, 12), it was found that the products did not have long-term room temperature stability. Apparatus for long-lasting intercalation compounds avoided such components (13). Reactors were usually constructed by joining $\frac{1}{4}$ in. FEP tubing (CHEMPLAST, Inc., Wayne, NJ 07470) or Pyrex tubing to a Teflon valve (previously described (17)). The samples of $(BN)_{\sim 3}SO_3F$ were prepared by condensing $S_2O_6F_2$ over BN such that the BN sample was completely immersed in the liquid $S_2O_6F_2$. For powder samples, the reaction was usually complete in half an hour and a deep blue product was obtained. Excess $S_2O_6F_2$ was removed in a dynamic vacuum (better than 10^{-3} Torr) and the dry product was further evacuated (10^{-3} Torr) for approximately 10 min. Samples of all preparations were taken for X-ray powder diffraction photographs (XRDP). If any unconverted *h*-BN was revealed by the XRDP, the solid was treated again with $S_2O_6F_2$ until conversion to the first-stage intercalation compound was complete. Compositions derived from gravimetry using powdered *h*-BN are given in Table 1. The X-ray powder data for $(BN)_{\sim 3}SO_3F$, and its unit cell, are given in Table 2.

For the HOPBN sample, the intercalation was done using liquid $S_2O_6F_2$ in a large glass reactor joined to a greaseless J. Young glass–Teflon valve. The center of the HOPBN sample was not yet completely blue after 2 days, but was deep blue after 3 days, some exfoliation of it having by then occurred. After 2 more days, the $S_2O_6F_2$ was removed. The HOPBN sample initially weighed 0.0640 g (2.58 mmol), and after the intercalation 0.187 g, indicating a composition of $(BN)_{2.1}SO_3F$. It is probable that the unacceptably high SO_3F content of the HOPBN intercalation compound derives from weighing error associated with the large glass reactor. Although the possibility that some double guest-layer intercalation had occurred cannot be ruled out with certainty, such additional intercalation has never been indicated in the work with powders, where, in any case, the intercalation proceeds very much more easily than in the HOPBN case. It is therefore probable that the true composition of the intercalated HOPBN was $(BN)_{\sim 3}SO_3F$.

TABLE 1
Gravimetric Data for the Synthesis of $(BN)_{\sim 3}SO_3F$

Sample	Weight BN (mg)	Weight product (mg)	x in $(BN)_xSO_3F$
BN + $S_2O_6F_2$ (l)			
	88.6	204.9	3.04
	101.9	235.3	3.05
	169.6	365.9	2.92
	173.3	407.0	2.96
	193.0	447.9	3.02
	246.4	578.4	2.96
BN + $S_2O_6F_2$ (g)			
2 h	107.3	211.7	4.11[a]
	125.8	230.4	4.80[a]
4 h	144.2	330.4	3.09

[a]X-ray powder pattern showed mixture of BN and $(BN)_xSO_3F$.

Instability of $(BN)_{\sim 3}SO_3F$ in apparatus with metal components (11, 12). Samples of *h*-BN (typically 50–200 mg) were loaded in Pyrex or fused silica tubes previously dried under vacuum at $\sim$200°C. Such tubes were each fitted with a stainless steel 1KS4 Whitey valve. The *h*-BN was fully

TABLE 2
X-Ray Powder Data (Cu$K\alpha$, Ni Filter) for $(BN)_{\sim 3}SO_3F$ with a Hexagonal Cell (a = 2.50(1) Å, c = 8.08(2)Å)

hkl	$1/d^2$ Calculated	$1/d^2$ Observed	Relative intensities
002	0.0612	0.0616	vs
003	0.1378	0.1378	m
100	0.2142	0.2158	s
004	0.2450	0.2479	m
005	0.3828	0.3830	w
110	0.6425	0.6413	m
111	0.6578	0.6539	vm
112	0.7038	0.7054	vvw
200	0.8564	0.8567	vw
210	1.4992	1.4992	w

TABLE 3
Gravimetric Data for the Decomposition of $(BN)_{\sim 3}SO_3F$ (Prepared and Contained in a Steel-Valved Tube) at $\sim 20°C$ under Vacuum

Initial composition	$(BN)_{3.07}SO_3F$	$(BN)_{3.04}SO_3F$	$(BN)_{3.0}SO_3F$
Initial wt. (mg)	123.8	249.1	276.3
Final wt. (mg) (25 h evac)	68.4	140.9	150.4
% Wt loss of product[a]	44.7	43.4	45.6

[a]A 43.7% weight reduction is required for the following decomposition: $6(BN)_3SO_3F_{(s)} \rightarrow 17BN_{(s)} + 5/2S_2O_5F_{2(g)} + NOSO_3F_{(s)} + 1/2B_2O_{3(s)}$.

immersed in liquid $S_2O_6F_2$ that was vacuum distilled into the tube at $-78°C$. Within 30 min at $\sim 20°C$ the solid was deep blue. After removal of surplus $S_2O_6F_2$ (5–10 min in a vacuum (10^{-3} Torr), when all liquid had been removed), the gravimetry indicated (12) the starting compositions given in Table 3. Each of the samples prepared and contained in this way was exposed to a dynamic vacuum (10^{-3} Torr) for 25 h at $\sim 20°C$. The volatile products were caught in a trap at $-196°C$ and examined by IR spectroscopy (Monel metal cell). This showed only the bands characteristic (18) of $S_2O_5F_2$. XRDP of the colorless solid product showed the pattern of poorly crystalline *h*-BN (this having been absent in the freshly prepared deep-blue $(BN)_{\sim 3}SO_3F$) and also the pattern of $NO^+SO_3F^-$. (The latter salt was prepared separately from NO and $S_2O_6F_2$ for the purpose of this identification.)

Stability of $(BN)_{\sim 3}SO_3F$ in a sealed Pyrex glass tube. A powder sample $(BN)_{\sim 3}SO_3F$ was prepared in a $\frac{1}{4}$ in. Pyrex tube with a Teflon valve. After the reaction was complete and excess $S_2O_6F_2$ (confirmed by IR (19) to be $S_2O_5F_2$ free) had been removed, the Pyrex tubing was drawn down and sealed under vacuum. There was no visible color change in this sealed sample over several months.

Instability of $(BN)_{\sim 3}SO_3F$ in liquid aHF. $(BN)_{\sim 3}SO_3F$ (33 mg) was loaded into a one-arm $\frac{1}{4}$ in. FEP reactor inside the DRILAB. $S_2O_6F_2$ (~ 0.1 ml) was vacuum transferred to the $(BN)_3SO_3F$ and the amount of liquid $S_2O_6F_2$ was sufficient to cover the $(BN)_{\sim 3}SO_3F$ solid. Then, aHF (~ 1.5 ml), dried over K_2NiF_6, was condensed into the reactor. As this mixture was warmed up to room temperature, the deep blue $(BN)_{\sim 3}SO_3F$ quickly started to loose its color. In approximately 2 h, the solid product was colorless. The liquid phase was tinged slightly yellow. The IR spectrum of the vapor indicated only $S_2O_6F_2$ (19) and HF (20).

Stability of $(BN)_{\sim 3}SO_3F$ toward HF vapor and moisture. HF vapor (~ 100 Torr) was introduced into the $\frac{1}{4}$ in. FEP reactor containing freshly made $(BN)_{\sim 3}SO_3F$. There was no obvious change in the appearance or color of $(BN)_{\sim 3}SO_3F$ over ~ 24 h. The reactor was evacuated and brought into the DRILAB, and a strand of quartz wool was inserted. HF vapor (~ 100 Torr) was added to generate a trace amount of H_2O via interaction with the SiO_2. There was some discoloration at the surface of the $(BN)_{\sim 3}SO_3F$, but the bulk of the solid remained deep blue and was still blue after 2 weeks.

Magnetic susceptibility dependence on temperature. A 14.5-mg sample of newly prepared $(BN)_{\sim 3}SO_3F$ was loaded into an air-tight Teflon capsule inside the DRILAB. The capsule was sealed and then suspended by a thread in a Quantum Design Magnetic Property Measurement System (MPMS) incorporating a superconducting quantum interference device (SQUID) magnetometer. Magnetization was measured as a function of temperature from 2 to 300 K. The magnetic gram susceptibility, x_g, was found to be 55.2×10^{-6} cgs units and this value remained constant over the entire temperature range.

Conductivity measurement on the HOPBN/SO_3F sample. The intercalated HOPBN sample was used for a four-point probe conductivity measurement. It was sandwiched between two Teflon sheets and an opening was cut in the top Teflon sheet for the probes. A series of data points was obtained of voltage vs a steady current applied using a PAR model M273 potentiostat/galvanostat (Princeton Applied Research). Because of the nature of its layered structure, $(BN)_{\sim 2.1}SO_3F$ was expected to be conductive in the BN sheets (*ab* plane) and the conductivity low along the *c* axis. The four sharp osmium probes were pressed through the entire thickness of the sample. The specific conductivity at a given temperature was calculated by the equation for a two-dimensional metal (21):

$$\rho = (\pi/t \ln 2)(V/i) \approx 4.54\ (V/i)/t. \qquad [3]$$

The extrapolated slope of voltage vs current data points was used for (V/i) in the calculation. The dimensions of the rectangular sample were $l = 10.40$, $w = 5.53$, thickness, and $t = 0.785$ mm. The measurement of the specific conductivity at room temperature was done inside the DRILAB with electrical leads connecting the four-point probe device to the potentiostat and voltmeter outside the DRILAB. The temperature-dependent conductivity measurements were made using a well-dried Pyrex apparatus. It had a top and bottom part, sealed by a standard glass O-ring joint. The four electrical leads and a thermocouple wire were passed through, fused into the top, and connected with the four-point probe device on the bottom of the apparatus, and the thermocouple tip was placed just beneath the sample. The bottom section of the apparatus was wrapped with heating tape and inserted snugly into a Pyrex beaker. This arrangement was immersed in liquid nitrogen and the temperature was regulated by a Eurotherm 808 temperature controller connected to the thermocouple and heating tape.

TABLE 4
X-ray Powder Diffraction Data (Cu*K*α, Ni Filter) for $C_{\sim 7}SO_3F$ with a Hexagonal Cell *a*=2.457(3) Å; *c*=7.727(5) Å

hkl	$1/d^2$ Calculated	$1/d^2$ observed	Relative intensities
001	0.0167	0.0169	mw
002	0.0669	0.0675	vs
003	0.1507	0.1509	s
B		0.2233	s
C		0.2554	vw, br
004	0.2679	0.2881	w
005	0.4186	0.4188	vw
110	0.6627	0.6626	w
111	0.6795	0.6795	w
112	0.7301	0.7338	vw
113	0.8134	0.8114	vw
210	1.5464	1.5470	vw

Note. *B* and *C* are probably 10*l* diffuse scattering associated with a nestled structure akin to that of $C_{14}AsF_6$ (30).

Graphite intercalation by $S_2O_6F_2$. Samples of small-crystallite graphite (SP1 Union Carbide) in contact with excess liquid $S_2O_6F_2$ for 2 h were converted wholly to first-stage material. Gravimetry for preparations that had been subjected to a dynamic vacuum ($\sim 10^{-3}$ Torr) to constant weight had a composition $C_{\sim 7.5}SO_3F$; the XRDPs of which are represented by the data in Table 4. Intercalation of pieces of HOPG, suitable for conductivity measurements, proceeded more slowly and were usually less complete than the powder.

Conductivity of HOPG/SO_3F. A HOPG sample ($\sim 5 \times 5 \times 0.5$ mm) contained in a rectangular cross-section quartz tube with a cavity ~ 5 times the thickness of the sample (the *z* axis direction for the graphite) and only slightly larger in the other dimensions was treated with excess liquid $S_2O_6F_2$ at 50°C for 1 h. Removal of $S_2O_6F_2$ under dynamic vacuum to constant weight indicated a composition for the sample of $C_{\sim 8.3}SO_3F$. The sealed quartz tube was cooled to 77 K and quickly inserted in the magnetic field of a Zeller contactless conductivity assessment device (22), with which $\sigma_{77K} \approx 3.1 \times 10^5\ S\,cm^{-1}$ and $\sigma_{295K} \approx 1.1 \times 10^5\ S\,cm^{-1}$. A comparison measurement on HOPG itself gave $\sigma_{295K} = 2.2 \times 10^4\ S\,cm^{-1}$.

Reactions of h-BN with PF_5/F_2, AsF_5/F_2, O_2AsF_6, and SbF_5. Interaction of *h*-BN, at ~ 20°C, with gaseous PF_5 or AsF_5 (each ~ 10 atm), or with liquid SbF_5, the mixture being vigorously agitated, failed to produce any intercalation. When F_2 was added to the PF_5 or AsF_5 (to ~ 5 atm F_2) small quantities of BF_3 were formed, but no intercalation occurred. Agitation with solid O_2AsF_6 similarly failed to bring about intercalation of the *h*-BN.

Intercalation of h-BN by SbF_5/F_2 mixtures. Mixtures of *h*-BN, SbF_5, and F_2 in 6:2:1 molar ratio in a stainless steel reactor with a Whitey KS4 value were agitated at ~ 0°C for 6 h. Some BF_3 was produced. Removal of volatiles left a light blue solid, the XRDP of which indicated the presence of a hexagonal first-stage salt with *a* indistinguishable from that of *h*-BN and $c = 8.01$ Å. Some unintercalated *h*-BN remained. Several preparations gave similar results and material entirely free of *h*-BN was never obtained.

Interaction of $(BN)_{\sim 3}SO_3F$ with AsF_5. $(BN)_{\sim 3}SO_3F$ was treated with AsF_5 (pressure 8 atm) at ~ 20°C in a *stainless steel reactor*. $S_2O_5F_2$ was evolved as AsF_5 was taken up, and on the third treatment with AsF_5 no further sulfur oxyfluoride evolution was detected. XRDP indicated the dark blue first-stage salt to be hexagonal with $a = 2.54\,(1)$ Å and $c = 8.25\,(2)$ Å (Table 5). Gravimetry was consistent with a product composition $(BN)_{\geq 9}AsF_5SO_3F$. A similar product was obtained using a 2:1 $AsF_5/S_2O_6F_2$ mixture on *h*-BN at ≤ 20°C. This salt was stable at least up to 100°C. Four probe (Pt wires) conductivity measurements on a pressed pellet indicated $\sigma_{293K} = 1.5\ S\,cm^{-1}$ and $\sigma_{100K} = 3\ S\,cm^{-1}$.

Interaction of $(BN)_{\sim 3}SO_3F$ with AsF_5/F_2. The previous experimental arrangement was repeated except for the inclusion of F_2 (1:2 with AsF_5). The volatiles expanded into an IR cell after 2 h were identified as $S_2O_5F_2$ and AsF_5 together with a trace of BF_3. After a further two cycles of AsF_5/F_2 treatment, no $S_2O_5F_2$ or $S_2O_6F_2$ was detected in the IR. The vacuum stable solid product was dark blue, and XRDP indicated that *h*-BN was absent, but, apart from weak lines attributable to $NOAsF_6$, was indistinguishable from that obtained by the action of AsF_5 alone on $(BN)_{\sim 3}SO_3F$. This solid showed no evidence of decomposition to 100°C. Conductivity measurements on a pressed pellet, at ~ 20°C indicated $\sigma_{293K} = 0.08\ (2)\ S\,cm^{-1}$, these low values being attributable to the insulating $NOSO_3F$ contaminant.

TABLE 5
X-Ray Powder Data for $(BN)_xAsF_5SO_3F$ (Cu*K*α, Ni Filter) with Hexagonal Cell (*a*=2.49 Å, *b*=8.25(2) Å)

hkl	$1/d^2$ Observed	$1/d^2$ Calculated	Relative intensities
001	0.0145	0.0147	M
002	0.0589	0.0588	S
003	0.1322	0.1324	M
100	0.2163	0.2136	M
004	0.2355	0.2353	WM
110	0.6402	0.6409	WM
111	0.6560	0.6566	WM
112	0.6993	0.6998	W

Interaction of h-BN with MF_6 ($M = Os, Ir, Pt$). In all cases the hexafluorides, which were condensed on to the finely divided *h*-BN, fluorinated the *h*-BN in highly exothermic reactions; at 0°C or below, boron trifluoride, lower fluorides (OsF_5, IrF_5, IrF_4 and PtF_4), and some metal were produced. In no case was there evidence of intercalation having occurred.

RESULTS AND DISCUSSION

In the early investigations (11, 12) of the product of interaction of *h*-BN with $S_2O_6F_2$ there was great variability in the stability of the $(BN)_{\sim 3}SO_3F$ with respect to evolution of $S_2O_5F_2$ and the formation of colorless solid products that were shown by XRDP to contain both *h*-BN and $NO^+SO_3F^-$. These identified products and the loss in weight that accompanied such decompositions (see Table 3) are consistent with the $S_2O_6F_2$ acting as an oxygen source according to the equation

$$6(BN)_{\sim 3}SO_3F_{(s)} \rightarrow 17BN_{(s)} + NOSO_3F_{(s)} + \tfrac{1}{2}B_2O_{3(c)} + \tfrac{5}{2}S_2O_5F_{2(g)}. \quad [4]$$

Evidently the $(BN)_{\sim 3}SO_3F$ is thermodynamically unstable with respect to these products. But some samples persisted without measurable decomposition for many months, whereas others decomposed within hours. When, in later work (13), steel, nickel, and other base metals were rigorously excluded from contact with the reagents, the $(BN)_{\sim 3}SO_3F$ product did not decompose over many months at ambient temperatures. It therefore appears that $(BN)_{\sim 3}SO_3F$ has kinetic stability at ordinary temperatures, but catalysts (so far undefined) can promote decomposition. The deliberate introduction of gaseous HF to a system free of base metals did not lead to as rapid a decomposition as when base metals were present. When the $(BN)_{\sim 3}SO_3F$ was immersed in liquid aHF at room temperature, however, its blue color faded completely in 2 h to give a colorless, poorly crystalline solid. In this case, the only volatile products were $S_2O_6F_2$ and HF. This is consistent with the interaction of HF with *h*-BN to make NH_4BF_4, as reported by Glemser and Haeseler (23), the overall reaction being

$$(BN)_{\sim 3}SO_3F_{(s)} + 12HF_{(l)} \rightarrow 3NH_4BF_{4(s)} + 1/2\ S_2O_6F_{2(g)}. \quad [5]$$

This instability of *h*-BN with respect to HF imposes a serious limitation to the preparative chemistry of *h*-BN intercalation compounds, since it is the only known ionizing solvent that is not oxidized by those reagents that are more powerfully oxidizing than $S_2O_6F_2$.

Electron affinities and intercalation. The molecule $S_2O_6F_2$ is in equilibrium with the $SO_3F^\bullet$ radical (19) at room temperatures, and it is the high electron affinity of this radical that is probably responsible for the facile intercalation of *h*-BN, and graphite, by $S_2O_6F_2$. Vibrational spectra of $FXeOSO_2F$ and $FXeOClO_3$ indicate that the binding of FXe– to $-OSO_2F$ is similar (16) to that with $-OClO_3$, from which it seems likely that the electron affinity $E(SO_3F^\bullet) \approx E(ClO_4^\bullet)$. The latter has been determined to be ≈ 134 kcal mol^{-1} (24).

It has been shown (25) that the oxidative intercalation of hexafluoroanionic species (MF_6^-) into graphite requires a threshold electron affinity of ~ 120 kcal mol^{-1}. The SO_3F^- species has the same effective thickness as MF_6^- (i.e., it requires the same separation of the graphite sheets, to ~ 8 Å); therefore, a similar electron affinity ought to apply to $SO_3F^\bullet$ because it easily generates first-stage graphite salts. On the other hand, $E(SO_3F^\bullet)$ cannot be as high as 153 kcal mol^{-1} because then SO_3F^- would be able to stabilize O_2^+ in $O_2^+SO_3F^-$ at 0°C, and it does not. The basis for this evaluation involves lattice energy, U, and entropy, S°_{298}, evaluations (26) for $O_2^+SO_3F^-_{(c)}$. Assuming the unit cell volume of O_2SO_3F to be close to that of KSO_3F, $U(O_2SO_3F) = -149$ kcal mol^{-1} and S°_{298} $(O_2SO_3F) = 39$ cal deg^{-1} mol^{-1} (26). For the reaction

$$O_{2(g)} + SO_3F^\bullet_{(g)} \rightarrow O_2^+SO_3F^-_{(c)}, \quad [6]$$

ΔS°_{298} must be ≈ -79 cal deg^{-1} mol^{-1} because S°_{298} values (27) for $O_{2(g)}$ and $SO_3F^\bullet_{(g)}$ (taken to be $\approx SO_2F_{2(g)}$) are ≈ 49 and 69 cal deg^{-1} mol^{-1}, respectively. From this $T\Delta S^\circ$ at 0°C ≈ -22 kcal mol^{-1}. So if the reaction as written is to be spontaneous at 0°C, ΔH° should be ≤ -22 kcal mol^{-1}. Given that $I(O_2) = 280$ kcal mol^{-1} (28) this would require $E(SO_3F^\bullet) \geq 153$ kcal mol^{-1}. But O_2^+ salts oxidize SO_3F^- even below 0°C (and this provides a basis for the preparation of $S_2O_6F_2$ (29)); therefore, the upper limit for $E(SO_3F^\bullet)$ can be set at 153 kcal mol^{-1}.

Because the late transition series hexafluorides (MF_6, M = Ru, Rh, Ir, and Pt) and the group 5 pentafluorides, in combination with F_2, have electron affinities (24) higher than that of SO_3F, it appeared probable that these oxidizers would also bring about *h*-BN intercalation. The metal hexafluorides, however, simply acted as potent fluorinating agents and no evidence of intercalation was observed, even when low reaction temperatures were employed.

Liquid SbF_5, with $F_{2(g)}$, was the only group 5 pentafluoride/F_2 combination with *h*-BN that brought about intercalation. Because there was always some fluorination of the *h*-BN (to generate BF_3) and there was never complete intercalation, the composition of the intercalation compound is not known. Since F_2 was needed for intercalation, however, we can be sure that anion formation $\{(SbF_5)_nF^-\}$ is essential to the intercalation process. The interlayer spacing of ≈ 8.01 Å is similar to that produced by the intercalation of hexafluoride species into graphite in a *nonnestled* way (30).

However, even $Sb_2F_{11}^-$, $Sb_3F_{16}^-$, and other chain-character anions derived from SbF_5 and F^- can also be accommodated in a gallery of this height, as long as the chains lie in a plane parallel to the BN sheets. The dark blue fluoroarsenate derivative, possibly $(BN)_yF_5AsOSO_2F$, made from $(BN)_{\sim 3}SO_3F$ was more stable than it (at least kinetically). That this intercalation compound was also preparable directly from *h*-BN and an $S_2O_6F_2/AsF_5$ mixture at $\sim 20°C$, as well as by the displacement of $S_2O_5F_2$ from $(BN)_{\sim 3}SO_3F$ by AsF_5, suggests that the guest species is $F_5AsOSO_2F^-$, a relative of the well-known superacid anion $F_5SbOSO_2F^-$ (31). The large interplanar spacing (8.25 (2) Å) is consistent with such an anion, which cannot be as easily close-packed as the SO_3F^- or MF_6^- species (25, 30).

Absence of higher stages in the h-BN intercalation compounds. The XRDP data for material of composition $(BN)_{\sim 3}SO_3F$ did not show lines of *h*-BN. Whenever less $S_2O_6F_2$ reagent was used in the synthesis than required for $(BN)_{\sim 3}SO_3F$, the lines of *h*-BN could be detected in the XRDP. No evidence for the existence of higher stages has ever been observed in the many preparations that have been carried out in these laboratories (11–13). This is in marked contrast to the graphite system, where the production of higher stage C_xSO_3F products was readily achieved (11) by limiting the supply of $S_2O_6F_2$ oxidant. This marked difference in intercalation behavior is probably associated with much diminished flexibility of the *h*-BN sheets compared with those of graphite. The excellent π bonding in the latter provides for the easy bending and warping required for the Daumas and Hérold domains (32) essential to higher stages of the graphite intercalation compounds. Such bending and warping in *h*-BN seems not to occur. Partial ionic character and poor π bonding in *h*-BN may be responsible for this.

Concerning the stoichiometry $(BN)_{\sim 3}SO_3F$ and comparison with $C_{\sim 7}SO_3F$. The *hk*0 reflections in the XRDP of $(BN)_{\sim 3}SO_3F$ indicate (see Table 2) that the apparent unit cell has a hexagonal unit cell parameter, $a \approx 2.50$ Å, not significantly different from that in *h*-BN itself. There is no firm evidence for a superlattice; therefore one must conclude that there is no ordered registry between the intercalant SO_3F^- species and the *h*-BN host. There are some *hkl* reflections (see Table 2) and these indicate that there might be an eclipsing of *h*-BN sheets, i.e., B over N, or like over like, with the SO_3F^- (in an unregistered array) between them. The separation of the BN sheets is 8.08(2) Å. This spacing immediately indicates (30) that the O and F ligands of the SO_3F^- guest are not nestled in the B_3N_3 rings, as are the guest ligands in the C_6 rings in $C_{\sim 7}SO_3F$. In the latter first-stage material the sheet to sheet spacing is ≈ 7.6 Å (see Table 4). This small value indicates that the SO_3F^- are nestled in the graphite sheets, in a manner akin to that of the AsF_6^- in $C_{14}AsF_6$ (30). This probably produces local order within a gallery but no order from one gallery to another, as in $C_{14}AsF_6$. Nestling of SO_3F^- requires the enclosing graphite layers to be staggered. The lines marked B and C (Table 4) may be a consequence of the random stacking of staggered graphite layers imposed by a nestled structure (30). The increase in the sheet to sheet spacing from *h*-BN, 3.33 Å, to that of $(BN)_{\sim 3}SO_3F$, 8.08 Å, gives an effective thickness of 4.75 Å for the guest species and a volume change, for each BN formula unit, of ~ 26 Å^3. The effective volume of the SO_3F^- species in $LiSO_3F$ (33) is ~ 81 Å^3. Therefore approximately three BN formula units are required for the accommodation of one SO_3F^- guest species. Clearly, from the stoichiometry, the SO_3F species must be close packed between the enclosing *h*-BN sheets, but there cannot be any registry between those of one gallery and those of adjacent galleries. Otherwise, *hk*0 superlattice reflections would have occurred.

Conductivity of $(BN)_{\sim 3}SO_3F$ and comparison with $C_{8.3}SO_3F$. In our early studies (12), a four-probe technique was employed, in which four platinum wires were used for electrical contact, and the samples were prepared by pressing powdered polycrystalline material into pellets. Because the platinum wires and the pellet surface are not ideally flat, a uniform intimate contact could not be assured between the wires and the pellet. The boundary effects due to the polycrystalline nature of the pellet sample also render such conductivity measurements unreliable. Attempts to use a contactless radio frequency inductive technique described by Zeller *et al.* (22) failed because this technique is not sensitive to low conductivities. A four-point probe measurement (21) on an intercalated highly oriented boron nitride sample was used in the present set of conductivity measurements. The $\sigma_{295K} \approx 1.5$ S cm^{-1}. The specific conductivity increased with decreasing temperature (see Fig. 1), it having nearly twice the room temperature value at 77 K. This indicates metallic behavior.

The metallic nature of the $(BN)_{\sim 3}SO_3F$ is also supported by the magnetic susceptibility which is that of a temperature-independent paramagnet over the temperature range 2–300 K.

The low value of the $(BN)_xSO_3F$ conductivity requires further comment. The room temperature specific conductivity of fluorosulfate-intercalated highly oriented pyrolitic graphite, with a composition of $C_{8.3}SO_3F$, was found to be $\sim 1.1 \times 10^5$ S cm^{-1}, which represents a five-fold increase over that of HOPG (2.0×10^4 S cm^{-1} at ~ 298 K). The charge carrier concentration in $C_{8.3}SO_3F$ should be comparable to that in $(BN)_{\sim 3}SO_3F$ if there is complete electron transfer to form SO_3F^- as the sole guest species in both materials. Although the conductivity measurements on the pellet of $(BN)_xF_5AsOSO_2F$ are less reliable than those on $(BN)_{\sim 3}SO_3F$, the observed σ values, for the compound prepared from AsF_5 interaction with $(BN)_{\sim 3}SO_3F$, are similar. The high vacuum stability of this material, even at

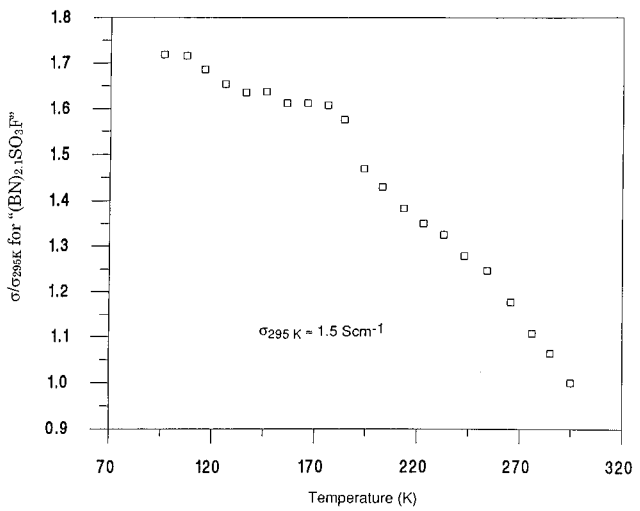

FIG. 1. Temperature dependence of the specific conductivity of a HOPBN/SO_3F sample: $(BN)_{2.1}SO_3F$.

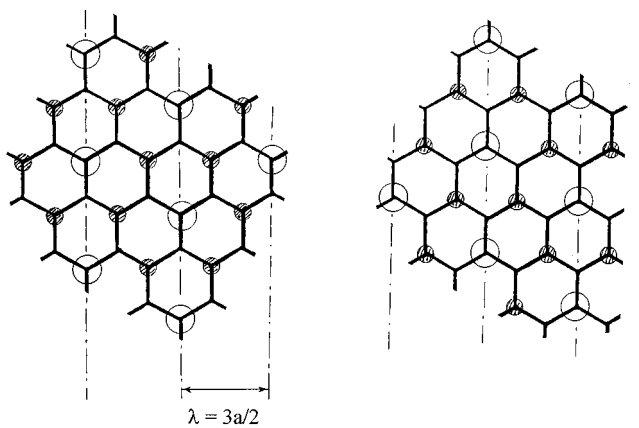

FIG. 2. The degenerate nonbonding crystal orbital combinations at each point (**P**) of the hexagon that defines the first Brillouin zone for a single graphite layer.

100°C, indicates that neutral guest species are unlikely to occur in it. The low conductivity of $(BN)_{\sim 3}SO_3F$ is therefore unlikely to arise simply from low charge carrier concentration.

The specific conductivity, σ, is related not only to the concentration of free charge carriers, n, but also to the mobility, μ, of the charge carriers (34):

$$\sigma = n_e\mu_e + n_p\mu_p. \qquad [7]$$

For graphite itself, the free charge carriers are produced as a result of a slight overlap of the conduction band and the valence band (35). The concentration of the free charge carriers is nevertheless small, and this characterizes graphite as a semi-metal. The high conductivity of graphite is a result of the very high mobility of the free charge carriers in that network. The mobility of the charge carrier (34) is related to the effective mass, m^*, of the carrier and the average time, τ, between scattering events for the carrier:

$$\mu = e\tau/m^*. \qquad [8]$$

Charge carriers with small effective mass behave as *light*, mobile particles, whereas *heavy* carriers with large effective mass have lower mobilities. In general, the charge carrier has a small effective mass in wide bands and a large effective mass in narrow bands. In the homonuclear system of graphite there is ideal combination of the p_z orbitals to give wide valence and conduction bands (36) (of essentially π character). In these bands, therefore, the charge carriers have high mobility. For a heteronuclear system, such as *h*-BN, the band width depends on the degree of interaction (or the overlap) between N and B orbitals, and inversely on the energy difference between the atomic orbitals. The energy difference between the B and N valence atomic orbitals is indicated by the large difference in first ionization potentials (28), I.P.(B) = 8.298 eV and I.P.(N) = 14.534 eV. Because the energy difference is large, the mixing of N and B atomic orbitals is small and the bands narrow. Therefore, in $(BN)_{\sim 3}SO_3F$ the charge carriers are *heavier* and less mobile than in the graphite system.

The charge carriers in $(BN)_x^+$ salts (holes in this case) are more likely to be confined on the boron sites. As has been pointed out in Ref. (37), this can be readily appreciated from a consideration of the nature of the *crystal orbital combinations* close to the Fermi level. In an isolated sheet of graphite (all carbon atoms equivalent), at 0 K (at the points **P** of the hexagonal first Brillouin zone of the hexagonal lattice), the valence and conduction bands share a degenerate pair of (nonbonding) *crystal orbital combinations* represented in Fig. 2. In a sheet of *h*-BN, the analogous *crystal orbital combinations* are no longer degenerate. That, with finite atomic p_z orbital contributions centered on nitrogen, must provide better binding energy for electrons than the *crystal orbital* with finite contributions at boron. The former is the highest energy *crystal orbital* of the valence band and the latter the lowest energy *crystal orbital* of the conduction band. In the oxidized *h*-BN compounds the vacant or partially filled orbitals of the valence band should have predominantly N p_z orbital character (i.e., electrons largely centered on nitrogen, positive holes on boron). This not only accounts for low mobility of the electrons in the cationic *h*-BN salts but also accounts for the band gap of $\sim$5.8 eV in *h*-BN (38). The latter also explains why both oxidative and reductive intercalation of *h*-BN is more difficult to achieve than for graphite.

ACKNOWLEDGMENTS

The authors are indebted to Dr. Arthur W. Moore of Union Carbide for his gifts of HOPBN and HOPG. They also gratefully acknowledge support from the National Science Foundation, Grant No. DMR-9404755, and the Director, Office of Energy Research, Office of Basic Energy Sciences, Chemical Science and Materials Science Divisions of the U. S. Department of Energy under Contract Number DE-AC-03-76SF00098. M.I. acknowledges support from the Hertz Foundation.

REFERENCES

1. R. S. Pease, *Acta Crystallogr.* **5,** 236 (1952).
2. R. C. Croft, *Aust. J. Chem.* **9,** 206 (1956).
3. W. Rudorff and E. Stumpp, *A. Naturforsch. Teil B.* **13,** 459 (1958).
4. A. G. Freeman and J. P. Larkindale, *J. Chem. Soc.* **A7,** 1307 (1969).
5. A. G. Freeman and J. P. Larkindale, *Inorg. Nucl. Chem. Lett.* **5,** 937 (1969).
6. K. Ohashi and T. Shinjo, *Bull. Inst. Chem. Res. Kyoto Univ.* **55,** 441 (1977).
7. C. Mugiya, N. Ohigashi, Y. Mori, and H. Inokuchi, *Bull. Chem. Soc. Jpn.* **43,** 287 (1970).
8. M. Sakamoto, J. S. Speck, and M. S. Dresselhaus, *J. Mater. Res.* **1,** 685 (1986).
9. N. Bartlett, R. N. Biagioni, B. W. McQuillan, A. S. Robertson, and A.C. Thompson, *J. Chem. Soc. Chem. Commun.* 200 (1978).
10. J. G. Hooley, Carbon **31** (3), 181 (1983).
11. R. N. Biagioni, Ph.D. thesis, University of California at Berkeley, 1980. LBL Report 11760.
12. S. Y. Mayorga, Ph.D. thesis, University of California at Berkeley, 1988. LBL Report 26132.
13. C. Shen, Ph.D. thesis, University of California at Berkeley, 1992. LBL Report 35162.
14. A. W. Moore, *Nature* **221,** 1133 (1969).
15. S. M. Williamson, *Inorg. Synth.* **12,** 147 (1968).
16. M. Wechsberg, P. A. Bulliner, F. O. Sladky, R. Mews, and N. Bartlett, *Inorg. Chem.* **11,** 3063 (1972).
17. B. Zemva, R. Hagiwara, W. J. Casteel, Jr., K. Lutar, A. Jesih, and N. Bartlett, *J. Am. Chem. Soc.* **112,** 4846 (1990).
18. A. Simon and R. Lehmann, *Z. Anorg. Alleg. Chem.* **311,** 224 (1961).
19. F. B. Dudley and G. H. Cady, *J. Am. Chem. Soc.* **79,** 513 (1957).
20. K. Nakamoto, "Infrared and Raman Spectra of Inorganic Coordination Compounds," Wiley, New York, 1986.
21. F. M. Smits, *Bell System Tech.* J. **37,** 711 (1958).
22. C. Zeller, A. Denenstein, and G. M. T. Foley, *Rev. Sci. Instrum.* **50**(5), 602 (1979).
23. O. Glemser and H. Haeseler, *Z. Anorg. Allg. Chem.*, **279,** 1415 (1959).
24. V. N. Medeneyev, L.V. Gurvich, V. N. Konrat'yev, V. A. Medvedev, and YE. L. Frankevich, "Bond Energies, Ionization Potentials and Electron Affinities," St. Martin's, New York, 1966.
25. N. Bartlett, F. Okino, T. E. Mallouk, R. Hagiwara, M. Lerner, G. Rosenthal, and K. Kourtakis, *in* "ACS Advances in Chemistry Series" (M. K. Johnson *et al.*, Eds.), Vol. 226. Am. Chem. Soc., Washington, DC, 1990.
26. C. Shen, R. Hagiwara, T. E. Mallouk, and N. Bartlett, *in* "ACS Symposium Series," Vol. 555 p. 26. Am. Chem. Soc., Washington, DC, 1994.
27. Janaf Tables. Dow Chemical Co., Midland, MI, 1977.
28. R. D. Levin and S.G. Lias, "Ionization Potential and Appearance Potential Measurements, 1971–1981," NSRDS-NBS71. U.S. Dept. of Commerce, Washington, DC, 1982.
29. A. Šmalc, *Inorg. Synth.* **29,** 10 (1992).
30. F. Okino and N. Bartlett, *J. Chem. Soc. Dalton Trans.* 2081 (1993).
31. G. A. Olah, G. K. S. Prakash, and J. Sommer, "Superacids." Wiley, New York, 1985.
32. N. Daumas and A. Hérold, *C.R. Acad. Sci. Ser. C* **268,** 373 (1969).
33. Z. Zak and M. Kosicka, *Acta Cryst. B* **24,** 1968 (1982).
34. P. A. Cox, "The Electronic Structure and Chemistry of Solids," Oxford Science Pubs., Oxford, New York, 1987.
35. J. W. McClure, *Phys. Rev.* **108,** 612 (1957); G. S. Painter and D. E. Ellis, *Phys. Rev. B* **1,** 4747 (1970); R. R. Haering, *Can. J. Phys.* **36,** 352 (1958).
36. J. W. McClure, IBM J. **July,** 255 (1964); M. S. Dresselhauss and J. G. Mauroides, *IBM J.* **July,** 262 (1964).
37. Reference 31, pp. 114–118.
38. A. Zunger, A. Katzir, and A. Halperin *Phys. Rev. B* **13,** 5560 (1976).